

A Unified 3D CFD Model for Jet and Pool Fires

Chenthil Kumar K.¹, Anil Kumar K. R.¹ and Amita Tripathi²

¹Fluidyn Consultancy (P) Ltd, 146, Ring Road, 5, HSR Layout, Bangalore – 560102, India

²Fluidyn France, 7 Boulevard de la Liberation, Saint Denis-93200, France

In general, a fire accident involves various processes such as evaporation of fuel from a pool, formation of jets, laminar and turbulent diffusion, diffusion controlled and kinetics controlled reactions, smoke and soot formation and thermal radiation. The increased computational power enables use of more accurate CFD based models of these processes for large scale fire simulations. This work presents some results of the development and validation of a 3D CFD based model for dispersion of fuel vapours and associated fire hazards. In general, fires occur in a wide range of flow regimes. Unifying the simulation of this wide range of flow under a single combustion model is a challenge. In the present work, a unified model to deal with flames in different regimes such as slow pool fires and fires due to low speed laminar and high speed turbulent jets is implemented by modifying the eddy dissipation concept (EDC) model to include the effect of local laminar or turbulent burning velocities properly. Also, the local flame surface area, which determines local reaction rate, is estimated in a way such that the effect of discretization (mesh size) on the average reaction rate is minimal in order to obtain results which are reasonably grid independent. Spatial distribution of different quantities, such as temperature, mixture fraction, velocity and species concentrations are computed and compared with the experimental measurements available in relevant literature. It is found that the developed model using with an identical set of parameters was able to capture the qualitative behaviour of all the flames with a reasonably good quantitative comparison.

Keywords: pool fire, jet fire, modified eddy dissipation concept

1. Introduction

A number of fire-related accidents in industries are driven by jet or pool fires. A jet fire, characterised by a high momentum flow, might impinge on nearby equipment such as storage vessels (Cleaver et al, 2003, Roberts, 2004) with extensive damage. The pools fires usually happen from fuel spillages and tank explosions and are also relatively common among industrial accidents. Therefore, risk assessments must include a fair estimate of the consequences related to fires and require thus simulations as accurate as possible. Accidental fires involve various physical processes such as pool evaporation, formation of jets, laminar and turbulent diffusion, diffusion controlled and kinetics controlled reactions, smoke and soot formation and thermal radiation. Use of computational fluid dynamics for the fire modelling has increased during the last few decades mainly due to the improved computational power. Numerical simulations can be based on the Reynolds-averaged Navier–Stokes (RANS) equations or the Large Eddy Simulations (LES) (Novozhilov, 2001). In general, the turbulent combustion models, which calculate reaction rate using turbulent length and time scales alone, may not be able to model the fires in the laminar regimes. However, using Arrhenius model along with sufficiently fine mesh to resolve the local flame structure may be too expensive for modelling large scale fires. Therefore unifying the simulation of this wide range of flows under a single combustion model is beneficial. In the present work, such a model is implemented by modifying the EDC (Eddy Dissipation Concept) model (Magnussen and Hjertager, 1976) to include the effect of local laminar or turbulent burning velocities properly. Also, the local flame surface area, which determines local reaction rate, is estimated in a way such that the effect of discretization (mesh size) on the average reaction rate is minimal in order to obtain results which are reasonably grid independent. Spatial distribution of different quantities, such as temperature, mixture fraction, velocity and species concentrations are computed and compared with the experimental measurements available in relevant literature. It is found that the developed model using an identical set of parameters was able to capture the qualitative behaviour of all the flames with a reasonably good quantitative comparison. The first part of this article will describe the numerical model developed with the CFD software, fluidyn-VENTIL. The second part will present validation cases for a wide range of flame regimes. These flames correspond to various types of fires such as burning of slow (a few cm/s) and high speed (~ 100 m/s) fuel jets and pool fires.

2. Model Description

The flow is considered to be viscous and either steady or unsteady. The thermodynamic properties of the fluid are calculated based on the mixture properties of gas mixtures. The density of the fluid is calculated with the ideal gas equation based on the pressure, temperature and the overall molecular weight of the gas mixture. The variation of specific heat with temperature is considered. The variation of viscosity, thermal conductivity and mass diffusivity with respect to the temperature are considered. Combustion is modelled using single step reactions in terms of fuel and oxidiser. Turbulence is modelled using the standard SST-k- ω model. The gas radiation losses are accounted using the P1 radiation model.

2.1 Hydrodynamic model

The flow and heat transfer in the gas phase is described by a finite volume (FVM) discretization of the three-dimensional governing equations, which include the Navier-Stokes equations for laminar and/or turbulent flow and the conservation equations of mass, energy and species. The discretization of the domain is done with a non-uniform unstructured mesh. The meshing tool integrated with the numerical solver automatically generates fine mesh in the regions of interest such as near the jet inlet or a pool surface or any obstacles. Pressure is computed using a Poisson solver for the pressure correction using SIMPLEC technique and density is computed from an equation of state. The 2nd order accurate convection schemes are used. Under influences of gravity, the density differences give rise to turbulence production or destruction. Turbulence production due to buoyancy is also evaluated and accounted for.

2.2 Combustion model

The modified EDC combustion model is used to predict the jet and pool fire behaviours. The EDC combustion model was modified to predict the laminar flame as well as high turbulent flame. The chemical reaction in the Fuel–Air mixture is assumed to take place through a one-step global reaction of the form as follows;



The reaction rate for the one step standard eddy dissipation reaction model is computed using the model according to Magnussen and Hjertager(1977) as

$$\omega_{EDC} = A\rho \frac{\varepsilon}{k} \min \left[Y_{Fuel}, \frac{Y_{O_2}}{\nu}, \frac{BY_p}{1 + \nu} \right] \quad (2)$$

In the present modification of the EDC flame model ε/k is replaced by $A_g \times u_t$ per unit volume (Arntzen, 1998). A_g is the grid flame surface area and u_t is turbulent burning velocity for the particular fuel –air mixture. This formulation with appropriate evaluation of A_g was found to produce results, which are grid independent to some extent, for premixed flames. Hence it is adopted in the current model for fires with the non-premixed flames also. Equation (2) is modified as

$$\omega_{MEDC} = A\Gamma_K \rho A_g u_t \min \left[Y_{Fuel}, \frac{Y_{O_2}}{\nu} \right] \quad (3)$$

where Γ_K is the flame quench factor, which is more important in the turbulent dominant jet flames. The flame quench factor Γ_K is calculated according to the model suggested by Bradley et al (1994). The mixture fraction transport equation is solved additionally and reproduced the equivalence ratio field to calculate the laminar burning velocity from the dispersed mixture strength. From the laminar burning velocity the turbulent burning velocity (Arntzen, 1998) is calculated and used for the reaction rate calculations.

2.3 Thermal radiation model

In order to facilitate the solution of the radiation transport equation (RTE), the following assumptions are usually made: wavelength dependence of radiation properties is ignored (grey gas) or the RTE is solved for specific bands. Scattering is neglected throughout the domain. Surfaces are assumed to be either grey-diffuse ($\varepsilon = \kappa a$ and $\varepsilon + \rho = 1$) or perfect specular reflectors. The RTE equation is solved using the P1 radiation model. P1 radiation model is based on the expansion of the radiant intensity, I , into an orthogonal series of spherical harmonics. The total absorption coefficient of the gas phase is the sum of the contribution of soot (Kent and Honnery, 1990) and combustion products (Magnussen and Hjertager, 1977).

$$\kappa_g = 1862 f_v T + 0.1 (X_{CO_2} + X_{H_2O}) \quad (3)$$

where f_v is the soot volume fraction, T is the gas temperature, and X_{CO_2} and X_{H_2O} are the volume fractions of carbon-dioxide and water vapour, respectively.

2.4 Soot Model

The integral soot model proposed by Moss and Stewart (1998) is used with the inclusion of the process of nucleation, heterogeneous surface growth and coagulation. The above mentioned soot model solves transport equations for soot volume fraction, f_v , and soot number density, n_d .

3. Numerical Model Validation

In the present work the developed fire model is tested for flames in five widely different flow regimes: (1) laminar diffusion (2) turbulent diffusion (3) partially premixed turbulent flame (4) partially premixed high speed jet flame and (5) buoyancy controlled diffusion. The first four cases represent jet fires with possible strong entrainment of air and the last case is representative of a pool fire, where the flow is driven mainly by buoyancy. The first three cases represent flames for low to moderate jet velocities and the fourth case have fuel jet velocities of the range of 100 m/s. Present study considers both the very low laminar flame speed fire (CH_4 -air mixture) and the very high laminar flame speed fire (H_2 -air mixture). In all the cases, except the fourth, the fuel is methane; in the fourth case it is hydrogen.

3.1 Laminar Diffusion Flame

The objective of this study is to simulate the laminar diffusion fire and compare the numerical results with the experimental measurements of gas temperatures by Ndubizu et.al (1998). Figure 1.(a) shows the Wolfhard-Parker burner experiment setup (Ndubizu et.al 1998) and Figure 1(b) is the simplified two-dimension numerical domain. In the experiment the average exit velocity of fuel is 0.0281 m/s and the average exit velocity of air is 0.181 m/s. The burner fuel inlet dimension is 0.01 m and the air inlet half width is 0.035 m. Due to symmetric domain, one half of the 2D domain is considered for the numerical simulation. The symmetric condition is imposed at centre of the domain. The uniform inlet velocities are considered for the fuel and oxygen as velocity inlet boundary conditions. Pressure static boundary conditions are applied on surroundings and outlets. The non-uniform meshes of 19500 elements are considered for the numerical simulation. The grid was refined close to the inlets and the minimum grid size was 0.2mm. Figure 2 and Figure 3 show the comparisons of numerically predicted temperature distributions at different heights along one side from centre with the experimental measurements. Figure 4 shows the contours for the gas temperatures and resultant velocity on the symmetric plane $y=0$.

3.2 Turbulent Diffusion Jet Flame

In this case a turbulent diffusion flame is simulated and the numerical results are compared with the experimental gas temperature measurements by Saqr et. al (2010). Figure 5(a) shows the experimental setup (Saqr et. al, 2010) and Figure 5(b) shows the simplified numerical domain. In the experiment methane is injected through a 4 mm diameter nozzle, into a 1 m long burner. The mass flow rate of methane and air are 1.72×10^{-4} kg/s and 1.18×10^{-2} kg/s, respectively. A 2D axis-symmetric computational domain is considered for the present numerical simulation. Pressure static boundary conditions are applied on cylindrical enclosures and outlets. The velocity inflow boundary conditions are imposed on the fuel and oxygen inlets. The symmetric boundary is imposed at the axis. The non-uniform meshes of 57584 elements are considered for the numerical simulation. The grid was refined close to the inlets and the minimum grid size was 0.3mm. Figure 6 shows the comparison of numerically predicted temperature distributions along the axis. Figure 7 shows radial temperature distribution at height of 0.3 m. Figure 8 shows the contours for the gas temperatures and resultant velocity on the symmetric plane $y=0$.

3.3 Partially Premixed Turbulent Jet Flame

In this case a turbulent, partially premixed, diffusion flame is simulated and compared numerical results with the experimental measurements of temperature, velocity and species concentrations by Barlow et al (2005). The experimental configuration is that of Sandia Flame D (Barlow et.al, 2005). Figure 9(a) shows the experimental setup (Barlow et.al, 2005) and Figure 9(b) shows the simplified numerical domain. The fuel inlet, pilot flame, and wind tunnel velocities are 49.6 m/s, 11.4 m/s and 0.9 m/s, respectively. The inlet temperatures of the main jet, pilot flame and the co-flow are 294 K, 1880 K and 291 K, respectively. For the jet, the inlet molar concentrations of methane and air are 0.25 and 0.75, respectively. A 2D axis-symmetric computational domain is considered for the present numerical simulation. The non-uniform meshes of 57584 elements are considered for the numerical simulation. The grid was refined close to the inlets and the minimum grid size was 0.3mm. The experimentally observed velocity profile is specified at the fuel inlet. Figures 10-13 show the comparison of numerically predicted axial temperature, axial velocity, axial fuel mass fraction and axial oxygen mass fraction with the experiment (Barlow et.al, 2005). Figure 14 shows the contours for the gas temperatures and resultant velocity on the symmetric plane $y=0$.

3.4 Partially Premixed High Speed Jet Flame

This case involves simulation of a high speed jet flame (Cabra et.al, 2002). Figure 15(a) shows the experimental setup (Cabra et.al, 2002) and Figure 15(b) shows the simplified numerical domain. The flow consists of a central H_2 and O_2 lifted jet flame within a coaxial flow of vitiated gases from a lean H_2 -air co-flow flame. The fuel inlet and co-flow velocities are 107m/s and 3.5m/s, respectively. The inlet temperatures of the main jet and the co-flow are 305 K and 1045 K, respectively. For the jet flow, the inlet molar concentrations of H_2 , O_2 , H_2O and air are 0.2537, 0.7427, 0.0021 and 0.0015, respectively. For the co-flow, the inlet molar concentrations of H_2 , O_2 , H_2O and air are 0.0005, 0.7532, 0.1474 and 0.0989, respectively. A 2D axis-symmetric computational domain is considered for the present numerical simulation. The non-uniform meshes of 22464 elements are considered for the numerical simulation. The grid was refined close to the inlets and the minimum grid size was 0.3mm. Figures 16 and 17 show the comparison of

numerically predicted axial temperature and mixtures fraction with the measurement. Similarly, Figures 18 and 19 show comparison of axial fuel and product mass fractions, respectively. Figure 20 shows the contours for the gas temperatures and resultant velocity on the symmetric plane $y=0$.

3.5 Buoyancy Controlled Diffusion Flame

In this case a buoyancy controlled diffusion flame is simulated and the temperature, mixture fraction and velocities are compared with the experimental measurements by Zhou et al (1998). Figure 21(a) shows the experimental setup (Zhou et al,1998) and Figure 21(b) shows the simplified numerical domain. This problem is similar to a pool flame. The flame is established on a diffuser burner with an exit diameter of 0.071 m. The fuel, methane, burns in a quiescent ambient air in an open environment. The fuel flow rate is 84.3 mg/s. Due to symmetry, one fourth of the domain is considered for the numerical simulation. Velocity inlet boundary conditions are applied at fuel inlets. The static pressure boundary condition is imposed at the outlet and surroundings. The fuel inlet velocity and temperature are 0.0314 m/s and 288 K, respectively. The uniform meshes of 38437 elements are considered for the numerical simulation. The uniform grid size was 2.8mm. Figures 22 and 23 show the comparison of numerically predicted temperature and mixture fraction at $H/D=0.14$ with the measurement. Figures 24 and 25 show the comparison of numerically predicted vertical and horizontal velocities at $H/D = 0.56$ and $H/D = 0.42$ along one side with the measurements. Figure 26 shows the contours for the gas temperatures and resultant velocity on the symmetric plane $X=0$.

4. Conclusions

An implicit, finite volume, non-uniform, unstructured, body fitting mesh based 3D CFD model to simulate accidental fires is developed. The model is integrated with models for ventilation, radiation and soot transport. The combustion model, using a modified eddy dissipation concept, is implemented such that it can simulate a wide range of flames that might occur in accidental fires. These regimes include (1) low speed laminar jet fires, (2) high speed turbulent jet fires and (3) slow buoyancy driven pool fires. This model, including that for soot and radiation, is used to simulate different flames in a wide range of regimes (from pool flames to high speed jet flames) and the results are compared with the measurements. It is found that the present model with the same set of parameters was able to capture the qualitative behaviour of all the flames with reasonably good quantitative comparison.

References

1. Arntzen., B. J., 1998, Modelling of Turbulent and combustion for simulations of gas explosion in complex geometries, *PhD Thesis*, The Norwegian University of Science and Technology, Division of Applied Mechanics, Thermodynamics and Fluid Mechanics.
2. Bradley, D., Gaskell, P. H. and Gu, X. J., 1994, Application of a Reynolds stress, stretched flamelet, mathematical model to computations of turbulent burning', *Combust. Flame*, 96: 221-248.
3. Barlow, R.S., Frank, J.H. , Karpetis, A.N. and Chen, J.Y., 2005, Piloted methane/air jet flames: Transport effects and aspects of scalar structure, *Combustion and Flame*, 143:433-449.
4. Cabra, R., Myhrvold, T., Chen, J.-Y., Dibble, R. W., Karpetis, A. N. and Barlow, R.S., 2002, Simultaneous laser Raman-Rayleigh-LIF measurements and numerical modeling results of a lifted turbulent H₂/N₂ jet flame in a vitiated coflow, *Proc. Combust. Instit.*, 29: 1881–1888.
5. Cleaver, R. P., Cumber, P. S. and Fairweather, M., 2003, Predictions of free jet fires from high pressure, sonic releases, *Combust. Flame*, 132: 463-474.
6. Kent, J. H. and Honnery, D. R., 1990, A soot formation rate map of a laminar ethylene diffusion flame, *Combust. Flame*, 79:287-298.
7. Magnussen, B. F. and Hjertager, B. H., 1976, On mathematical models of turbulent combustion with special emphasis on soot formation and combustion, *Sixteenth Symposium(International) on Combustion*, 719- 729.
8. Moss. J. B. and Stewart, J. B., 1998, Flamelet-based smoke properties for the field modeling of fires, *Fire safety journal*, 30:229-250.
9. Ndubizu, C. C., Ananth, R. and Tatem, P. A., 1998, On water mist fire suppression mechanisms in gaseous diffusion flame, *Fire Safety Journal*, 31:253-276.

10. Novozhilov, V., 2001, Computational fluid dynamics modeling of compartment fires, *Prog. Energy Combust. Sci.*, 27(6):611–666.
11. Roberts, T. A., 2004, Effectiveness of an enhanced deluge system to protect LPG tanks and sensitivity to blocked nozzles and delayed deluge initiation, *J Loss Prev Process Ind*, 17: 151-158.
12. Saqr, K. M., Ali H. S., Sies, M. M. and Wahid, M. A., 2010, Effect of free stream turbulence on NO_x and soot formation in turbulent diffusion CH₄-air flames, *International Communication in Heat and Mass Transfer*, 37: 611-617.
13. Zhou, X. C. and Gore, J. P., 1998, Experimental estimation of thermal expansion and vorticity distribution in a buoyant diffusion flame, *Proc. Combust. Inst.* 2:2767-2773.

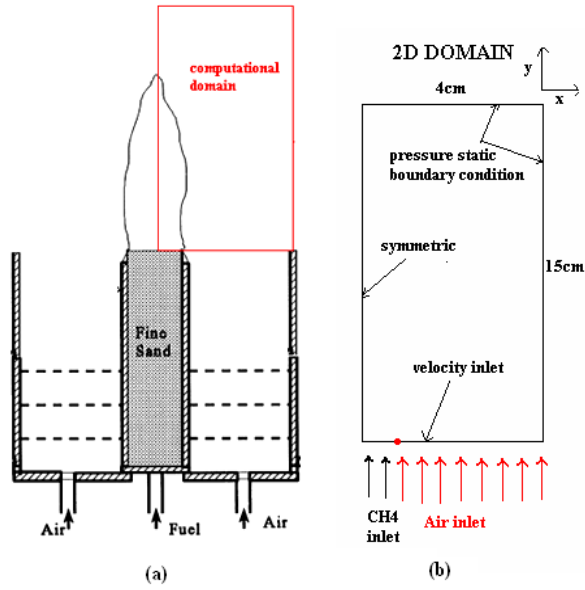


Figure 1: (a) Wolfhard- Parker burner (Ndubizu et.al, 1998); (b)2D Numerical domain

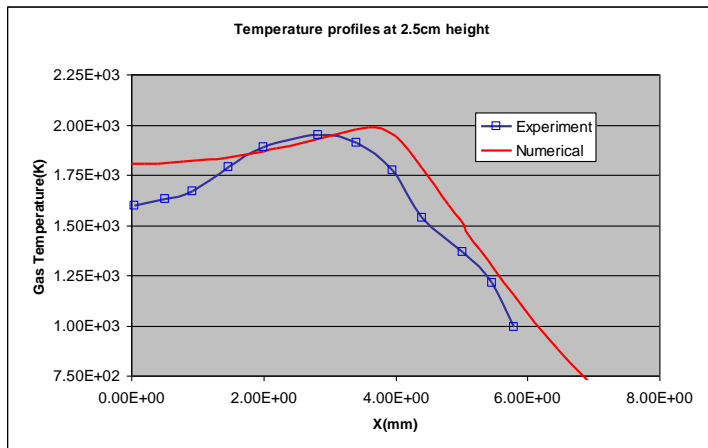


Figure 2: Comparisons of computed gas temperature with the measurement (Ndubizu et.al, 1998)

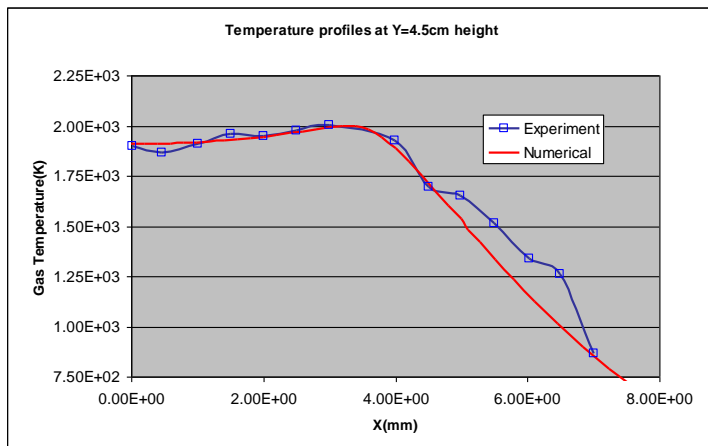


Figure 3: Comparisons of computed gas temperature with the measurement (Ndubizu et.al, 1998)

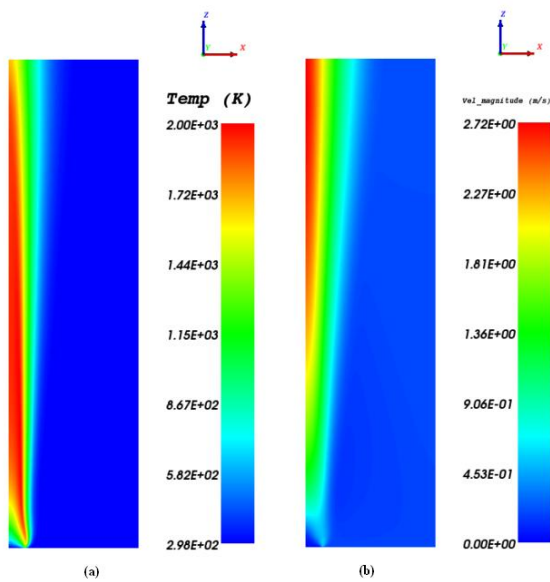


Figure 4: Contours on the symmetric plane Y=0 (a) Temperature contours (b) Resultant velocity contour

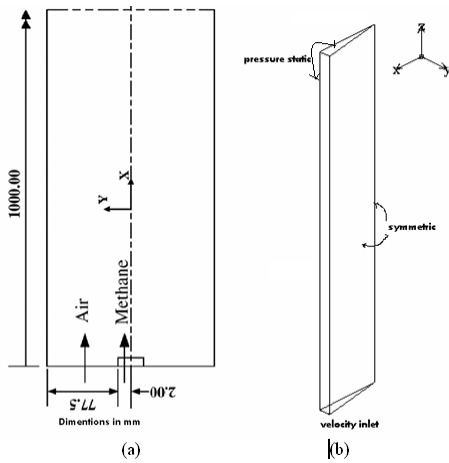


Figure 5: (a) Experiment setup (Saqr et. al, 2010); (b) Numerical domain

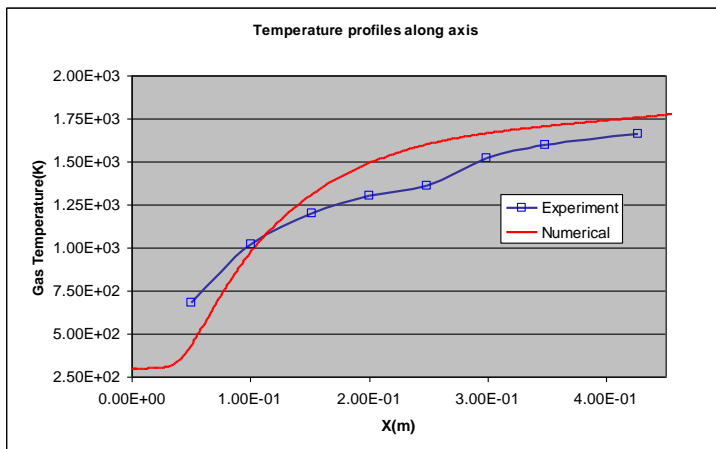


Figure 6: Comparison of computed gas temperature along axis with experiment Saqr et.al (2010)

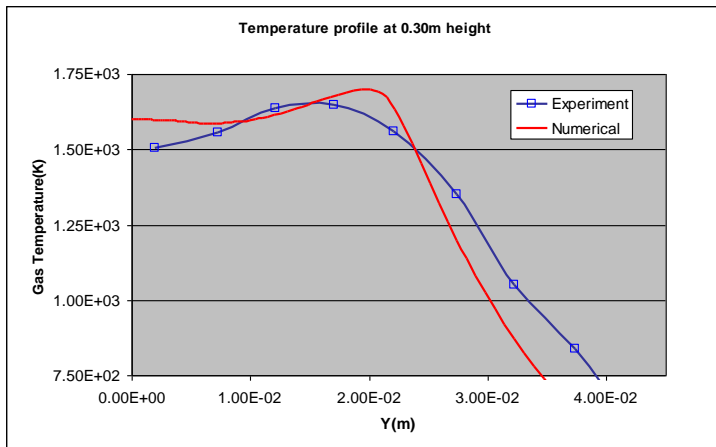


Figure 7: Comparison of computed gas temperature on height 0.3m with experiment Saqr et.al (2010)

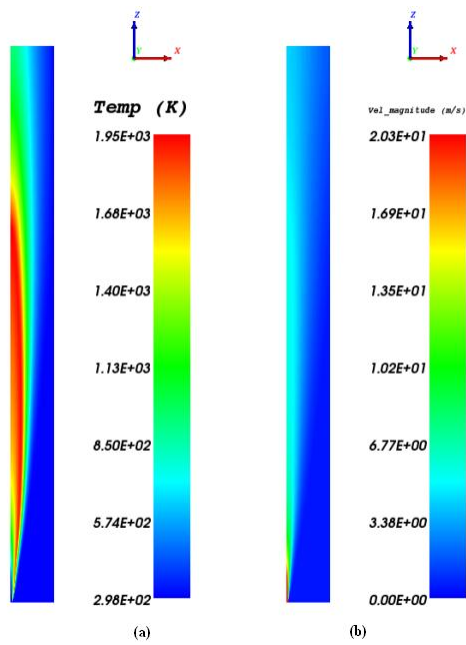


Figure 8: Contours on the symmetric plane Y=0 (a) Temperature contours (b) Resultant velocity contour

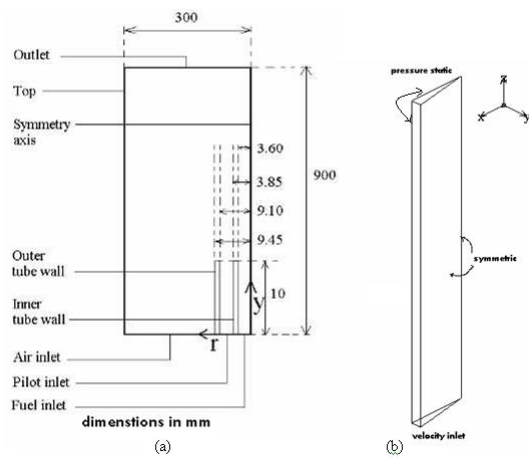


Figure 9: (a) Experiment setup (Barlow et.al, 2005); (b) Numerical domain

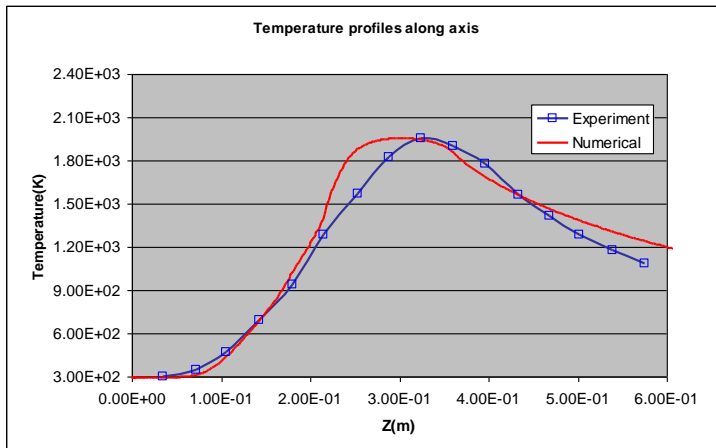


Figure 10: Comparison of computed temperature distribution with the experiment (Barlow et.al, 2005)

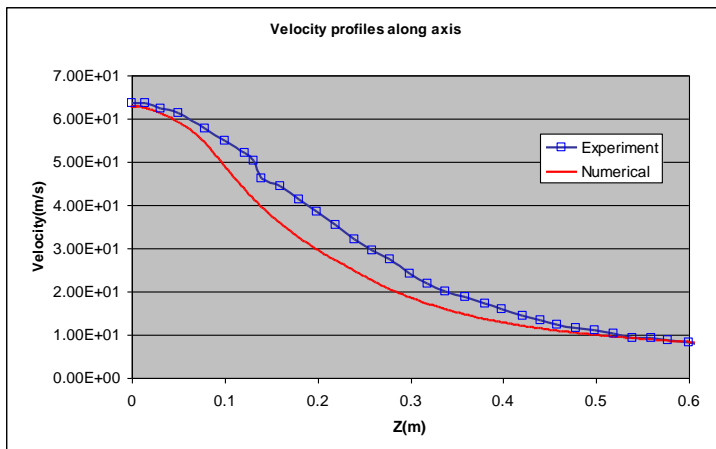


Figure 11: Comparison of computed velocity distribution with the experiment (Barlow et.al, 2005)

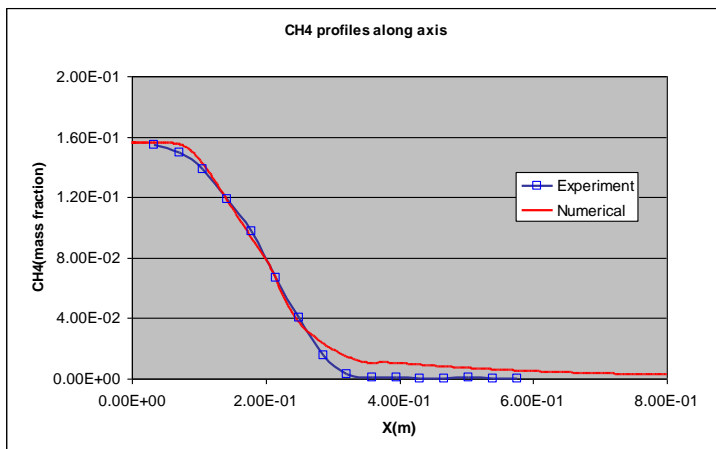


Figure 12: Comparison of computed fuel distribution with the experiment (Barlow et.al, 2005)

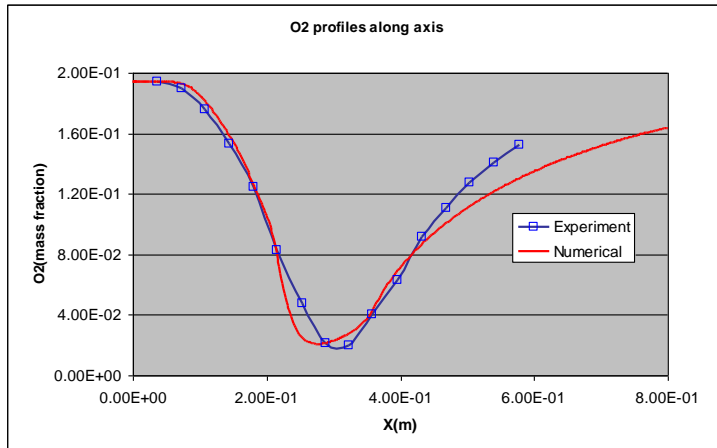


Figure 13: Comparison of computed oxygen distribution with the experiment (Barlow et.al, 2005)

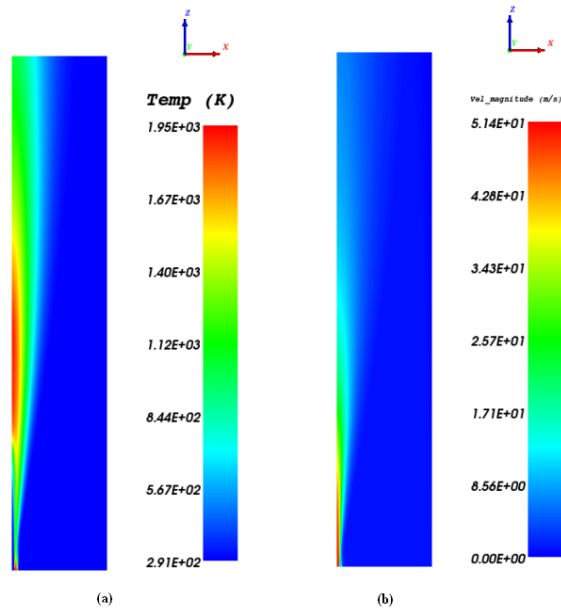


Figure 14: Contours on the symmetric plane Y=0 (a) Temperature contours (b) Resultant velocity contour

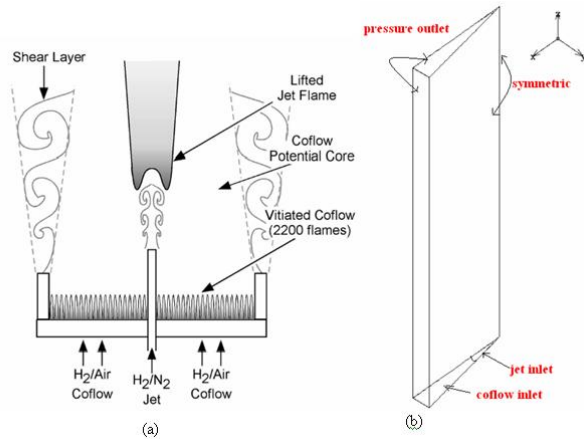


Figure 15: (a) Experiment setup (Cabra et.al, 2002); (b) Numerical domain

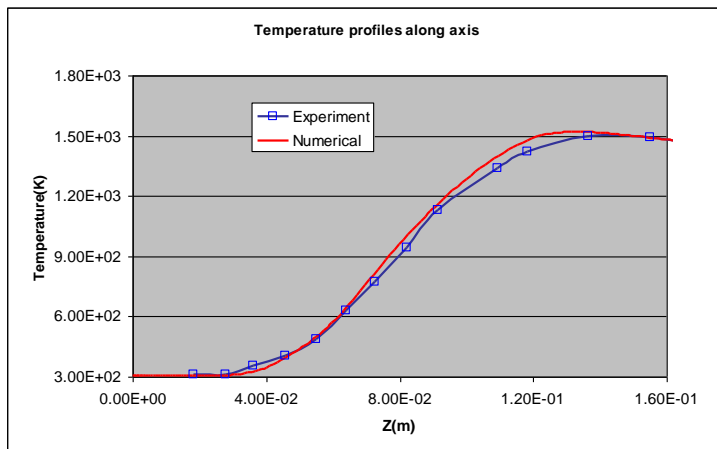


Figure 16: Comparison of computed temperature distribution with the experiment (Cabra et.al, 2002)

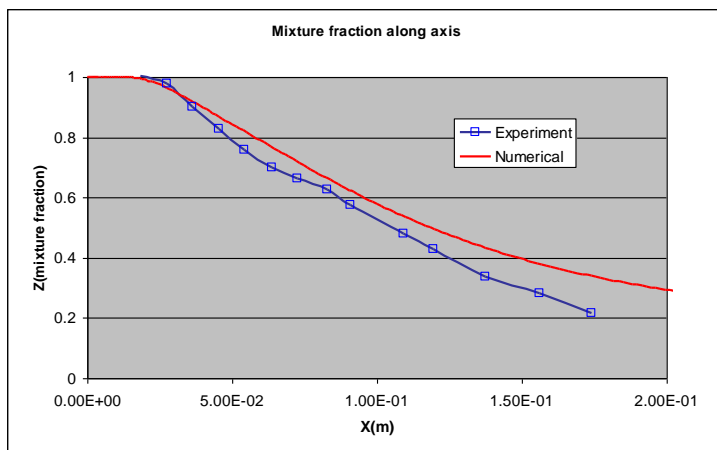


Figure 17: Comparison of computed mixture distribution with the experiment (Cabra et.al, 2002)

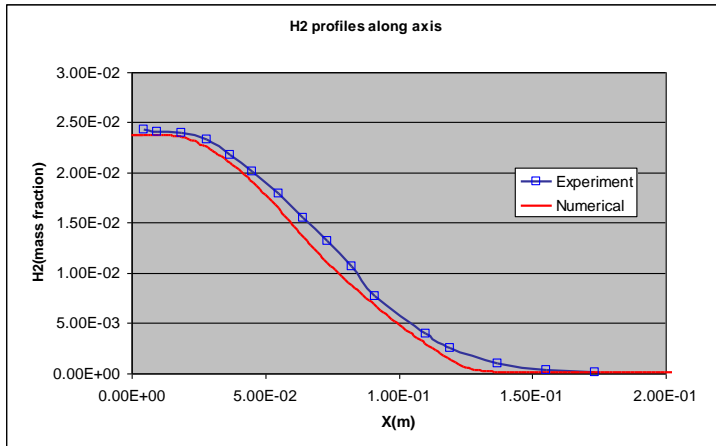


Figure 18: Comparison of computed fuel distribution with the experiment (Cabra et.al, 2002)

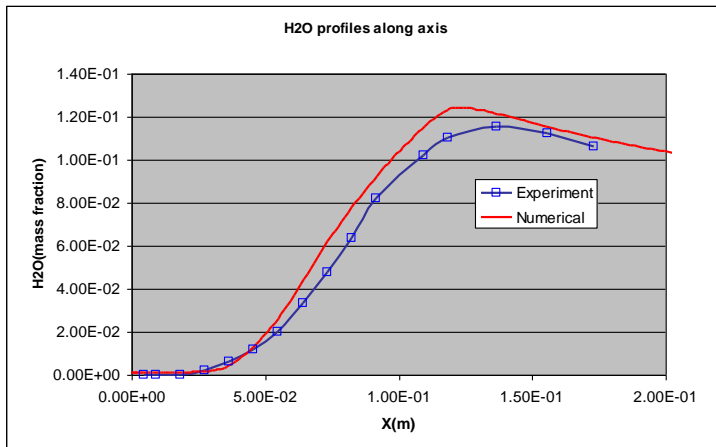


Figure 19: Comparison of computed product distribution with the experiment (Cabra et.al, 2002)

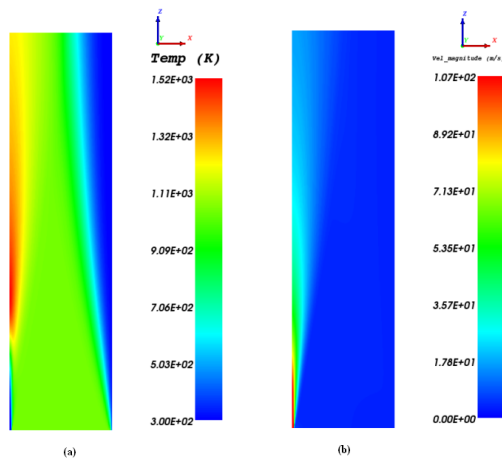


Figure 20: Contours on the symmetric plane Y=0 (a) Temperature contours (b) Resultant velocity contour

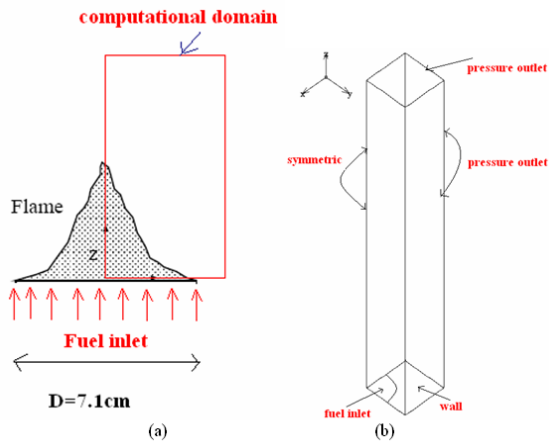


Figure 21: (a) Experiment setup (Zhou et al, 1998); (b) Numerical domain

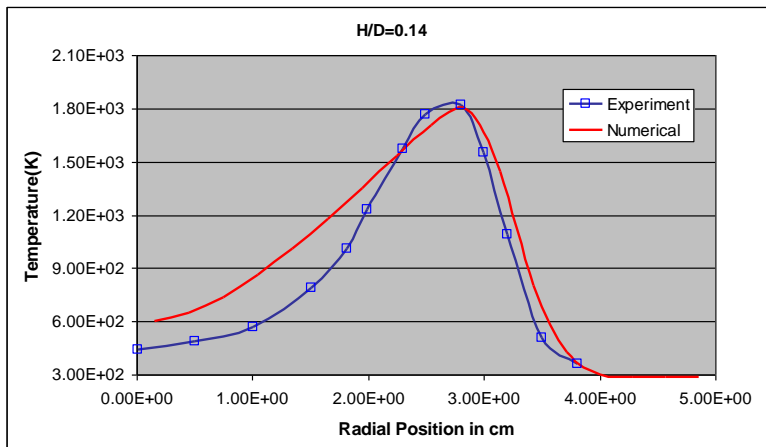


Figure 22: Comparisons of computed gas temperature with the experiment (Zhou et al, 1998)

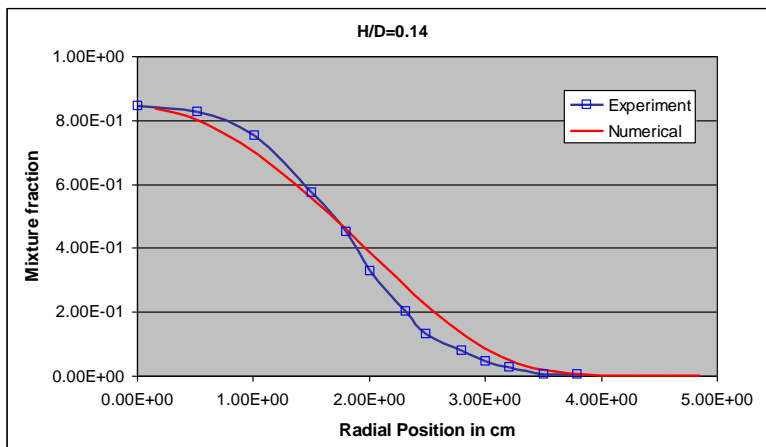


Figure 23: Comparisons of computed mixture fraction with the experiment (Zhou et al, 1998)

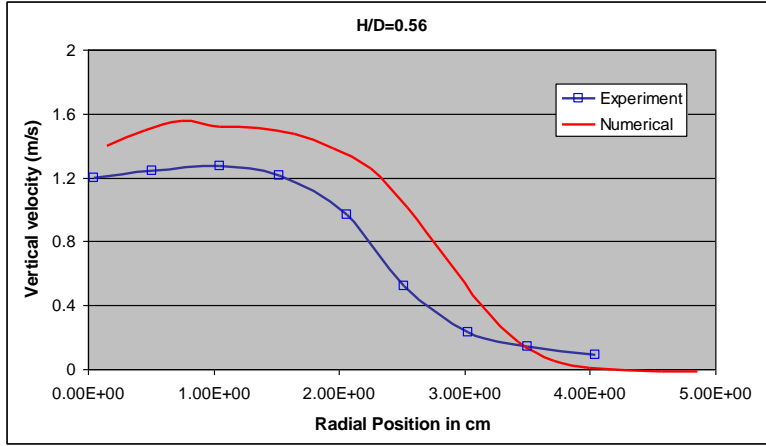


Figure 24: Comparisons of computed vertical velocity with the experiment (Zhou et al, 1998)

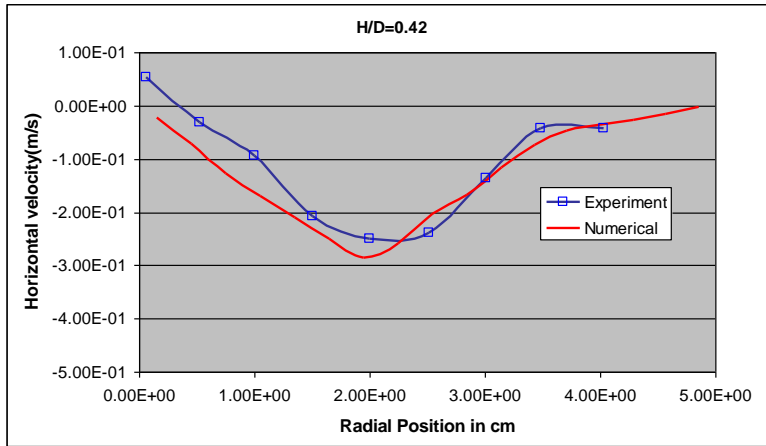


Figure 25: Comparisons of computed horizontal velocity with the experiment (Zhou et al, 1998)

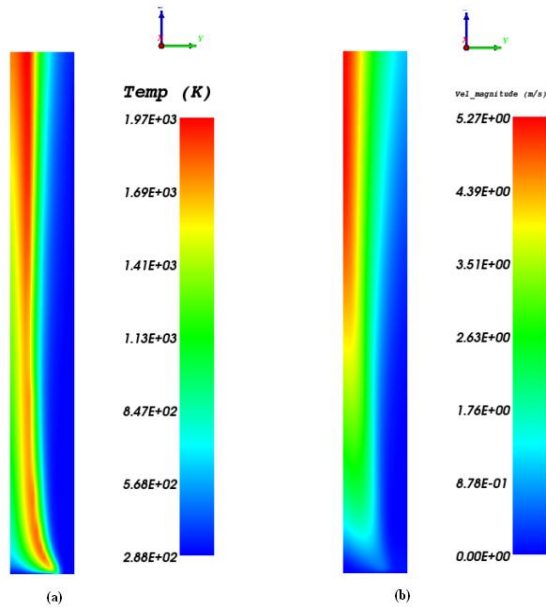


Figure 26: Contours on the symmetric plane X=0 (a) Temperature contours (b) Resultant velocity contour